

Article

Evaluation of Adsorption Efficiency on Pb(II) Ions Removal Using Alkali-Modified Hydrochar from *Paulownia* Leaves

Marija Koprivica * , Marija Simić , Jelena Petrović , Marija Ercegović  and Jelena Dimitrijević 

Institute for Technology of Nuclear and Other Mineral Raw Materials, Franchet d'Esperey 86, 11000 Belgrade, Serbia

* Correspondence: m.koprivica@itnms.ac.rs; Tel.: +381-64-271-3992

Abstract: In this study, hydrothermal carbonization (HTC) at five temperatures (180, 200, 220, 240, and 260 °C) was applied to transform *Paulownia* leaves (PL) into a carbonaceous sorbent of Pb(II) from aqueous solutions. To enhance the adsorption efficiency of the obtained hydrochar (PH), subsequent alkali activation was performed using NaOH. Preliminary results of the Pb(II) adsorption ($C_{Pb} = 200$ mg/L) showed removal coefficients after 48 h of 73.44 mg/g, 82.37 mg/g, and 110.9 mg/g for PL, PH-220, and MPH-220, respectively. The selected hydrochar (PH-220) and modified hydrochar (MPH-220) were further investigated by scanning electron microscopy (SEM) and Fourier transform infrared spectroscopy (FTIR). The results revealed that alkali treatment changed the hydrochar structure and, thus, improved its adsorption performance. The kinetic parameters showed that the Pb(II) sorption onto MPH-220 followed a pseudo-second-order model, while the intra-particle diffusion went through two simultaneous stages. The Langmuir isotherm model best described the experimental data and indicated the value of 174.75 mg Pb(II)/g as the maximum adsorption capacity. The two possible mechanisms of Pb(II) binding were complexation and/or Pb- π electron interaction. The obtained results indicate the great potential of MPH-220 for Pb(II) removal from aqueous media and its potential utilization as an effective adsorbent for wastewater purification.

Keywords: biowaste hydrochar; alkali modification; lead removal; kinetics and isotherm models; adsorption mechanism



Citation: Koprivica, M.; Simić, M.; Petrović, J.; Ercegović, M.; Dimitrijević, J. Evaluation of Adsorption Efficiency on Pb(II) Ions Removal Using Alkali-Modified Hydrochar from *Paulownia* Leaves. *Processes* **2023**, *11*, 1327. <https://doi.org/10.3390/pr11051327>

Academic Editor: Zongbi Bao

Received: 1 March 2023

Revised: 20 April 2023

Accepted: 23 April 2023

Published: 25 April 2023



Copyright: © 2023 by the authors. Licensee MDPI, Basel, Switzerland. This article is an open access article distributed under the terms and conditions of the Creative Commons Attribution (CC BY) license (<https://creativecommons.org/licenses/by/4.0/>).

1. Introduction

The HTC of biomass is a thermochemical conversion process, which contributes to the exploitation of residual waste in the form of valuable, low-cost, carbon-rich solid materials (hydrochars) [1,2]. Transformation of biomass during HTC takes place only in an aqueous mixture of biomass heated in a closed autoclave in a mild temperature range (180–250 °C) under autogenous pressure [3–5]. The fundamental advantages of HTC that exceed that of traditional biomass conversion methods include mild reaction conditions, the absence of gas evaporation, and the necessity for pre-drying biomass treatment. Due to the specificity of the structural features of the obtained hydrochars, the application of these materials has been scrutinized in numerous fields [4,6]. Since the structure of hydrochars is characterized by the presence of reactive oxygen functional groups (OFG) and increased aromaticity, one of the application fields includes the adsorption of various pollutants [3,5]. However, the influence of the small specific surface area of bare hydrochar limits the utilization of hydrochar as an adsorbent [7,8]. Therefore, to improve the reactivity of the obtained hydrochars, various physical and chemical activations have been applied [6,9–17]. The chemical methods show excellent performance for modified hydrochar, which was observed to be highly efficient for heavy metal removal [8,10]. Ordinarily, the increment in OFG content can be achieved by alkali treatment [11]. Furthermore, cold alkaline modification is low-cost and facile and, thus, is a promising method for industrial utilization [12,13].

Lead is a heavy metal with a highly negative impact on the environment and human health. Therefore, much attention has been directed toward the removal of this metal from

industrial effluents caused by mining activities and different industrial processing [6,12]. Previous studies showed that alkali-activated hydrochars derived from waste biomass could be successfully applied for Pb(II) removal [3,4,12,17]. Petrović et al. observed that the adsorption capacity of grape pomace hydrochar increased from 27.8 mg/g up to 137 mg/g after KOH activation [17]. Furthermore, Wang et al. demonstrated that ultrasound-assisted alkali activation resulted in more OFG, greater pore volume, and a larger surface area, which contributed to better sorption capacity of activated biochar [12]. Additionally, Rasam et al. showed that the efficiency and porosity of the final hydrochar adsorbent also depended on temperature and the residence time during the HTC process. From this study, the optimal hydrochar, with a specific area of 862.4 m²/g and adsorption capacity of 89.52 mg/g, showed 1.4 times better sorption of Pb ions compared to commercial activated carbon (64.18 mg/g) [3].

A waste biomass available in large quantities are the *Paulownia* leaves (PL) that remain after the *Paulownia* tree is used for timber and as an energy source. In our previous research, we studied in detail whether PL was suitable for HTC treatment. Although the obtained *Paulownia* hydrochar (PH) exhibited better combustion characteristics and higher energy content than the raw material, it did not show satisfactory energy yields due to the herbaceous leaf structure [18]. To examine another possibility for PL utilization, for the first time in the literature, we investigated the application of PH for heavy metal removal. The obtained PH was additionally alkali-activated with NaOH and utilized as a novel adsorbent of Pb(II) ions. A detailed examination of the adsorption process, with an emphasis on the binding mechanism of the pollutant, was undertaken. The different adsorption kinetic and isotherm models were applied to experimental data. Additionally, extensive characterization of the synthesized material by SEM and FTIR spectroscopy before and after adsorption was performed.

2. Materials and Methods

2.1. Chemicals

Sodium hydroxide (NaOH), lead (II) nitrate (Pb(NO₃)₂ × 3H₂O), potassium nitrate (KNO₃), nitric acid (HNO₃), potassium hydroxide (KOH), and potassium bromide (KBr, FT-IR grade) were procured from Merck (KGaA, Darmstadt, Germany). A stock solution of Pb(II) (2000 mg/L) was prepared by dissolving the proper amount of Pb(NO₃)₂ × 3H₂O in ultrapure water. Solutions of various Pb(II) concentrations used in the experiments were prepared by diluting the primary stock solution. All the chemicals were of analytical purity grade. Ultrapure water was used for the HTC process and solution preparations.

2.2. Material Preparation

The *Paulownia* leaves (PL) were collected from a park in Belgrade, Serbia, washed with ultrapure water, air-dried, and ground in order to obtain homogenous samples. A sieved fraction of 0.5 mm was used in HTC experiments.

The HTC process was performed in a laboratory 250 mL autoclave (Carl Roth, Model II). For the production of hydrochar, 10 g of the PL powder was stirred with 150 mL of ultrapure water at selected reaction temperatures (180, 200, 220, 240 and 260 °C) for 1 h. The obtained hydrochars (PH-180, PH-200, PH-220, PH-240 and PH-260) were separated from the liquids by filtration, rinsed three times with ultrapure water, and dried at 105 °C for 24 h.

Alkali modification was performed by stirring 5 g of the selected PH-220 with 500 mL of 2 M NaOH solution for 1 h at room temperature. The obtained activated hydrochar (MPH-220) was filtered, rinsed, adjusted to the neutral pH value, and dried overnight in an oven at 105 °C.

2.3. Preliminary Adsorption Test

For comparison and selection of the PH with the best adsorption capacity, PL, PH-180, PH-200, PH-220, PH-240, and PH-260 were used for the preliminary adsorption test.

A quantity of 0.08 g was mixed with 50 mL of Pb(II) solution (200 mg/L) for 48 h (at pH 5) at room temperature. After filtration, the Pb(II) concentrations in the residual solutions were determined using an atomic adsorption spectrophotometer (AAS, PerkinElmer, PinAAcle 900T).

The amount of Pb(II) ions adsorbed on the hydrochars was calculated using the following equation:

$$q = (C_0 - C_{eq})/m \times V \quad (1)$$

where q [mg/g] is the adsorbent capacity, C_0 and C_{eq} [mg/L] are the initial and subsequent adsorption concentration of Pb(II), m [g] is the amount of adsorbent and V [L] is the volume of the Pb (II) solution.

Additionally, 0.025 g of PH-220 and MPH-220 were mixed with 25 mL of Pb(II) solution (100 and 200 mg/L) at different times: 24 h, 32 h, 48 h, and 56 h. Furthermore, the efficiency of these samples for the removal of Pb(II) ions from wastewater was estimated using real effluent from the accumulator factory in Serbia. Metal concentrations (Pb, Cu, Zn, Cd, Ni, Fe) in wastewater before and after adsorption were measured using an AAS method.

2.4. Effect of Contact Time and Kinetics Studies

The effect of contact time on Pb(II) removal from aqueous solution using the selected MPH-220 was studied within a time period that ranged from 10 min to 48 h. For this experiment 0.025 g of the MPH-220 was mixed with 25 mL of the Pb solution (200 mg/L) for different contact times. The experimental data from this study were interpreted using three kinetic models (the Lagergren pseudo-first order (PFO) model, the pseudo-second-order (PSO) model, and the Weber–Morris intra-particle diffusion model):

The non-linear (Equation (2)) and linear (Equation (3)) Lagergren PFO rate equation [19–21] are:

$$q_t = q_{eq} \times (1 - e^{-k_1 t}) \quad (2)$$

$$\ln(q_{eq} - q_t) = \ln q_{eq} - k_1 t \quad (3)$$

Additionally, the non-linear (Equation (4)) and linear (Equation (5)) PSO rate equations [20,22] are:

$$q_t = q_{eq}^2 k_2 t / (1 + k_2 q_{eq} t) \quad (4)$$

$$t/q_t = (1/k_2 q_{eq}^2) + (1/q_{eq} \times t) \quad (5)$$

where q_{eq} and q_t [mg/g] are the amount of Pb(II) adsorbed by MPH-220 at equilibrium and the time t [min] is calculated from the kinetic models. The k_1 [1/min] and k_2 [g/mg min⁻¹] values are the pseudo-first-order and pseudo-second-order constant rates, respectively.

The Weber–Morris intra-particle diffusion model equation [23] is:

$$q = k_{id} t^{0.5} + C \quad (6)$$

where q [mg/g] represents the amount of adsorbed Pb(II) in time t [min], k_{id} [mg/g min^{-1/2}] represents the intra-particle diffusion rate constant, and C is the intercept.

2.5. Effect of Initial Metal Concentration and Isotherm Studies

Adsorption isotherms and ion-exchange studies were conducted by stirring 0.04 g of the MPH-220 and 40 mL of Pb solutions (pH 5.0) at different concentrations (0, 30, 50, 70, 100, 150, 200, 300, 400, and 500 mg/L), during 24 h. Isothermal modeling of the experimental results of the Pb(II) adsorption process on the MPH-220 surface was utilized using different isotherms (Langmuir, Freundlich, Sips, and Redlich–Peterson).

The Langmuir isotherm model considers a monolayer adsorption process onto a homogeneous media composed of distinct sites with constant adsorption energy. This isotherm model has been expressed by the following equation [24]:

$$q_e = q_m \times (K_L C_e) / (1 + K_L C_e) \quad (7)$$

where C_e [mg/L] is the equilibrium concentration, q_e and q_m [mg/g] represent the equilibrium and the maximum amount of the Pb adsorbed onto the MPH-220 surface, and K_L [L/mg] is the Langmuir constant related to the affinity of the binding sites.

The Freundlich isotherm model is based on the multilayer binding process onto a heterogeneous adsorbate surface with sites which have different adsorption energy. This model can be expressed in its non-linear form [25]:

$$q_e = K_F \times C_e^{1/n} \quad (8)$$

in which q_e [mg/g], K_F [(mg/g) (L/mg)^{1/n}], C_e [mg/L] and $1/n$ are the adsorption capacity at equilibrium, the Freundlich constant related to the adsorption capacity, the Pb(II) concentration at equilibrium, and the adsorption intensity, respectively.

The Sips model is a hybrid form of the Langmuir and Freundlich models, which predicts adsorption on a heterogeneous surface. At low concentration of sorbate, the Sips model is transformed to the Freundlich isotherm, while, at high concentration, it takes the form of the Langmuir isotherm (Equation (9)) [26]:

$$q_e = q_m \times (K_S C_e^{n_S}) / (1 + K_S C_e^{n_S}) \quad (9)$$

in which q_e and q_m [mg/g] represent the equilibrium and maximum adsorption capacity, K_S [L/mg] is the equilibrium constant, C_e [mg/L] is the equilibrium Pb(II) concentration, and n_S is the model exponent that varies between 0 and 1 [17], depending on the degree of uniformity on the adsorbent surface [15].

The Redlich–Peterson (RP) isotherm model proposes a homogeneous monolayer sorption process with constant adsorption energy and constant enthalpies. If the isotherm exponent (β) is close to 1, the RP model is converted into the form of the Langmuir isotherm, while, if its value is closer to 0, the RP model equation represents the reciprocal of the Freundlich isotherm [27,28]:

$$q_e = (K_{RP} C_e) / (1 + a_{RP} C_e^\beta) \quad (10)$$

where q_e [mg/g] and C_e [mg/L] are the adsorption capacity and Pb(II) concentration at equilibrium, respectively. K_{RP} [L/g] and a_{RP} [L/mg] are the RP model constant and equilibrium constant, respectively, while β represents the dimensionless exponent.

All the adsorption experiments were performed in triplicate; the average values of the obtained results are shown. To investigate the adsorption kinetics and isotherm models, linear and non-linear fitting methods were employed using Microsoft Excel 2010 and Origin 9.0 software. The correlation coefficient (R^2) and the chi-square test were used to identify the goodness of fit [29]:

$$\chi^2 = \sum_{i=1}^n (Q_i - q_i)^2 / q_i \quad (11)$$

where Q_i is the equilibrium capacity of the fitting model, while q_i is the equilibrium capacity from experimental data, and n is the number of preformed experiments. When Q_i and q_i have similar values, the value of χ^2 will be a small number.

2.6. Thermodynamic Studies

An investigation of the thermodynamic parameters (change in: Gibbs free energy ΔG° , enthalpy ΔH° , and entropy ΔS°) was conducted at three temperatures (298, 308, and 318 K) with different initial Pb(II) concentrations. The mixture of 0.025 g MPH-220 and 25 mL of the Pb solution was shaken for 24 h (pH = 5, 220 rpm). After filtration, the Pb(II)

concentrations in the initial and residual solutions were determined using an AAS device. The free energy change, ΔG° , was calculated by Equations (12) and (13) [20,30]:

$$\Delta G^\circ = -RT \ln K_c \quad (12)$$

$$\Delta G^\circ = \Delta H^\circ - T\Delta S^\circ \quad (13)$$

The van't Hoff equation was used in order to calculate the ΔH° and ΔS° parameters from the slope and intercept of the plot, respectively [20]:

$$\ln K_c = -\Delta H^\circ / R \times (1/T + \Delta S^\circ / R) \quad (14)$$

where T is the temperature [K], R is the universal gas constant [8.3144 J/(mol × K)], and K_c is the equilibrium constant. There are several approaches and ways of calculating the equilibrium constant K_c . The most common in the literature use the Langmuir constant (K_L), the Freundlich constant (K_F), the partition (K_p), or the distribution coefficient (K_d) [20]. In order to avoid mistake when calculating the K_c , the values of K_L [L/mg] were converted to dimensionless K_c according to Milonjić [30].

2.7. FTIR Analysis

FTIR analysis was used to determine the presence of functional groups on the surface of the PH-220 and MPH-220 before and after the Pb(II) sorption process. The FTIR analysis of the samples was recorded on a Thermo Fisher Scientific Nicolet IS-50 spectrophotometer in the spectral range of 400–4000 cm^{-1} in transmission mode. All samples were converted into pellet form using KBr.

2.8. SEM/EDS

The surface morphology of the PH-220 and MPH-220 before and after Pb(II) adsorption was observed using SEM analysis (JEOL JSM-6610LV SEM, JEOL Inc., USA). All samples were cathodic-coated with gold, placed on an adhesive carbon disc, and recorded in a vacuum under a voltage of 20 kV.

2.9. Ion-Exchange Study

To examine the contribution of possible ion-exchange mechanisms during the adsorption of Pb(II) ions, the content of released cations (H^+ , Ca^{2+} , Mg^{2+} , K^+ and Na^+) was measured in the residual solutions. The MPH-220, with ultrapure water at pH 5.0, served as a control sample to eliminate the potential influence of van der Waals forces and H^+ attachment under acidic conditions.

The concentrations of Pb^{2+} , Ca^{2+} , Mg^{2+} , K^+ , and Na^+ in the solutions before and after adsorption were determined using an atomic adsorption spectrophotometer (AAS, PerkinElmer, PinAAcle 900T, Waltham, MA, USA). The concentration of H^+ ions was determined by a digital pH meter AMT20 (Amtast, London, UK).

2.10. The Point of Zero Charge of MPH-220 Surface

A point of zero charge (pH_{PZC}) analysis of the MPH-220 was conducted by a pH drift method [29]. Briefly, a 0.01 M KNO_3 solution, and either HNO_3 or KOH , was used to adjust the pH values between 2 and 12. MPH-220 (0.1 g) was added to each initial solution (50 mL), the mixtures were shaken for 24 h, and the final pH values were recorded after filtration. The initial and final pH values (pH_i and pH_f) were used to identify pH_{PZC} as the point at which the values were equal ($\Delta\text{pH} = 0$).

2.11. Stability and Reusability Studies

The assessment of the chemical oxidation stability of the adsorbents was determined using the $\text{K}_2\text{Cr}_2\text{O}_7$ /sulfuric acid (H_2SO_4) oxidation method [31]. The proportion of carbon

loss, i.e., the amount of oxidized carbon with respect to the total carbon of the biochar, was estimated following (Equation (15)).

$$P_{\text{carbon}} = M_{\text{carbon}}/150 \times C_{\text{cb}} \quad (15)$$

where P_{carbon} is the proportion of carbon loss, M_{carbon} is the mass loss of carbon, and C_{Cb} represents the carbon content of the hydrochar.

The desorption test was carried out in a batch system. The MPH-220 (0.1 g) was added in 100 mL of 200 mg/L Pb(II) solution and the mixture was shaken for 240 min (220 rpm) at room temperature. The solid residue was separated by filtration, washed, and dried. After that, Pb loaded MPH-220 was mixed with 0.1 mol/L HNO₃ (100 mL) and shaken for 240 min (220 rpm) at room temperature. The mixture was filtered, washed with ultrapure water, dried and used in the next sorption/desorption run. Desorption tests were performed in three cycles. The adsorption capacities of the sorption (q_a) and desorption (q_d) were determined for each cycle. The desorption efficiency (d_E) was calculated using the following equation [29]:

$$d_E = (q_d/q_a) \times 100\% \quad (16)$$

3. Results and Discussion

3.1. Preliminary Adsorption Test

The preliminary adsorption test revealed that the feedstock and different PHs exhibited different adsorption abilities toward Pb(II) (Figure 1a). Since the PH-220 showed the best adsorption capacity compared to the other investigated hydrochars, this sample was chosen for alkali modification and further adsorption experiments.

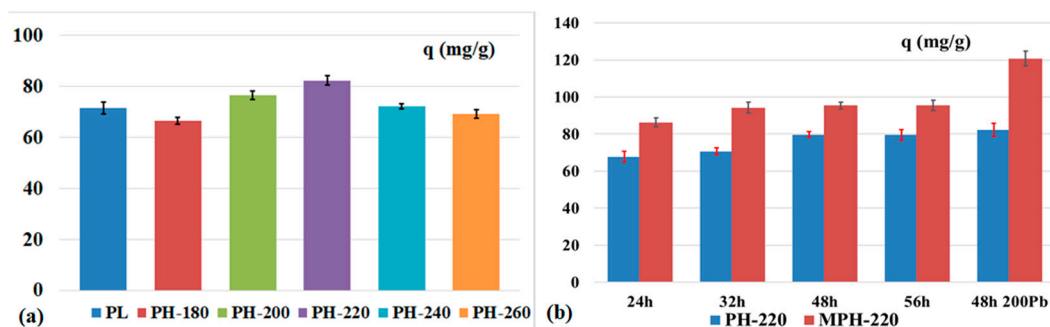


Figure 1. (a) Preliminary results of the Pb(II) adsorption (after 48 h); (b) Comparison of the adsorption capacities of PH-220 before and after alkali modification.

As can be observed in Figure 1b, alkaline modification improved the adsorption of Pb(II) ions. This effect was better observed when the concentration of lead in the aqueous solution was higher. The ability for sorption from wastewater, where many components can significantly impact efficiency, was also tested. For this purpose, real effluent (AFWW) from the accumulator factory was taken. The obtained experimental results are shown in Table 1. The MPH-220 reduced the concentration of Pb(II) ions and other detected ions in the wastewater better than the PH-220. The lower adsorption of metal ions compared to single metal removal data was probably caused by the solution's low pH (pH was 2). Nonetheless, MPH-220 exhibited good adsorption potential of the selected metal ions from industrial wastewater.

Table 1. Real wastewater before and after removal of metals by PH-220 and MPH-220.

	Pb (mg/L)	Cu (mg/L)	Zn (mg/L)	Cd (mg/L)	Ni (mg/L)	Fe (mg/L)
AFWW	5.71	8.22	4.27	1.35	4.72	7.85
AFWW-PH-220	5.02	7.85	3.87	1.11	3.96	7.21
AFWW-MPH-220	3.35	4.92	3.20	0.84	3.15	4.76

3.2. Effect of Contact Time and Kinetics Studies

The change in Pb ion concentration in the solution during the different periods was monitored (Figure 2). The results revealed that the MPH-220 rapidly removed the Pb ions in the initial stage but that this progressively slowed down until final equilibrium was reached. This observation was probably a result of the abundance of available active sites on the hydrochar surface at the initial stage [17,32]. After eight hours, a slower capacity increase was observed, and equilibrium was reached by approximately 24 h (Figure 2a). Additionally, retardation in the sorption capacity rate indicated that deposition played no significant role in the purge of Pb(II) ions [28].

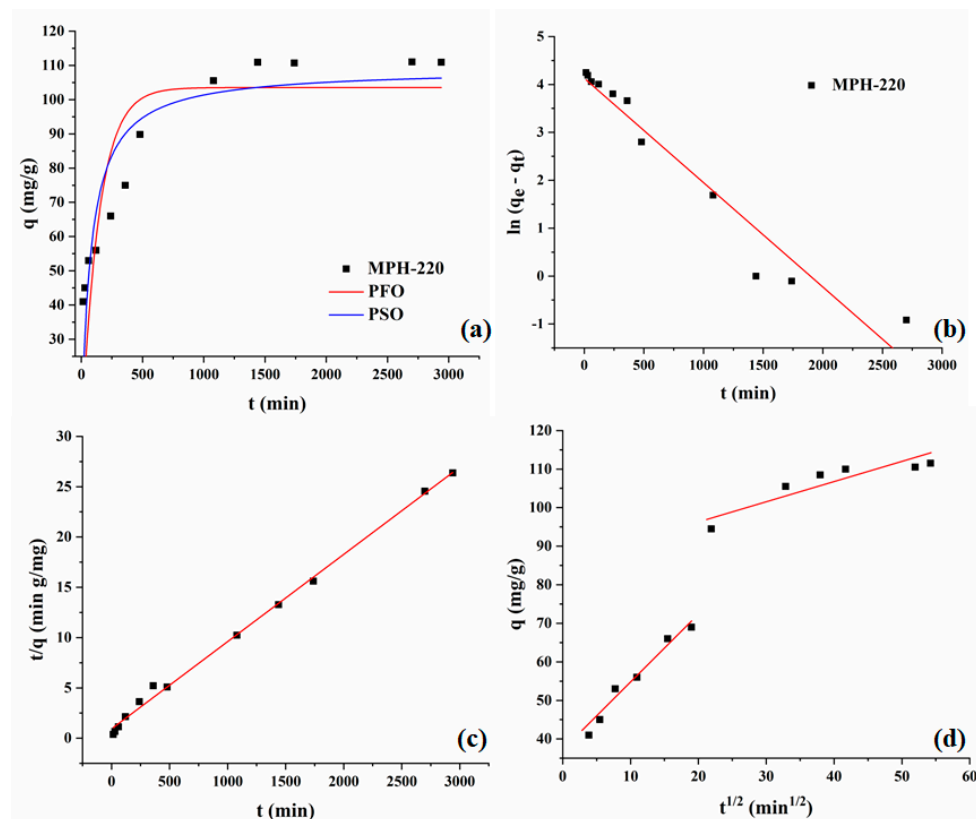


Figure 2. (a) Effect of contact time and applied non-linear kinetic models; (b) linear PFO model; (c) linear PSO model and (d) Weber–Morris intra-particle model for Pb(II) adsorption (200 mg/L) on the MPH-220.

To gain insight into the adsorption kinetics and Pb binding mechanism, non-linear and linear pseudo-first order (PFO) [19,20], non-linear and linear pseudo-second-order (PSO) [20,22], and intra-particle diffusion kinetic models were applied to the experimental data (Figure 2) [23]. The calculated parameters from Table 2 showed that the adsorption of selected metal ions onto the MPH-220 followed linear PSO kinetics ($R^2 = 0.9978$). Moreover, the calculated equilibrium adsorption value determined by the linear PSO model ($q_{eq,cal} = 113.34$ mg/g) was in agreement with the experimentally obtained result ($q_{eq,exp} = 110.9$ mg/g). This model implies that chemisorption played a major role during the sorption of Pb(II) ions by MPH-220. Similarly, previous investigations revealed that chemical interaction that involves covalent bonding and the exchange of electrons between Pb(II) ions and surface functional groups, is the rate-controlling step during adsorption by different modified hydrochars and biochars [4,7,8,12]. The experimental data are also explained using a non-linear form of the first-order (PFO) and second-order (PSO) kinetic models (Figure 2a, Table S1). Although the values of R^2 were smaller compared to the corresponding linear models, the non-linear kinetic parameters showed that the Pb(II) adsorption onto MPH-220 followed PSO ($R^2 = 0.9137$). A non-linear PSO kinetic model

has been observed in heavy metal sorption utilizing similar materials [33,34]. An applied Weber–Morris intra-particle model (Figure 2d) showed two different linear zones, indicating that intra-particle diffusion of metal ions was not the only rate-controlling step and that other mechanisms could be inferred too [15,28]. The first linear zone showed that the initial rapid sorption of metal ions occurred on the MPH-220 external surface, while the second linear zone indicated intraparticle diffusion followed by Pb(II) ions binding to the active sites [8,15,17,33,35]. In summary, the results from the kinetic study indicated that the removal of the Pb ions onto MPH-220 occurred through two simultaneous stages.

Table 2. Kinetic parameters of linear models for Pb(II) adsorption onto MPH-220, $C_{Pb} = 200$ mg/L.

Adsorbent MPH-220		
Pseudo-First-Order Model	$q_{eq,exp}$ [mg/g]	110.9
	$q_{eq,cal}$ [mg/g]	82.18
	k_1 [1/min]	0.0022
	χ^2	7.01
	R^2	0.9348
Pseudo-Second-Order Model	$q_{eq,cal}$ [mg/g]	113.34
	k_2 [g/(mg min)]	0.00008
	χ^2	5.27
	R^2	0.9978
	Weber–Morris diffusion Model	K_{id1} [mg/(g min ^{1/2})]
C_1 [mg/g]		35.64
R^2		0.9694
K_{id2} [mg/(g min ^{1/2})]		0.47
C_2 [mg/g]		87.82
R^2		0.8869

3.3. Sorption Isotherm Models

To examine the influence of the Pb(II) initial concentration on the removal efficiency of the sorbent, and to determine the maximum adsorption capacity, four isotherm models, Langmuir, Freundlich, Sips, and Redlich–Peterson were applied to the experimental data. The results are shown in Table 3 and Figure 3.

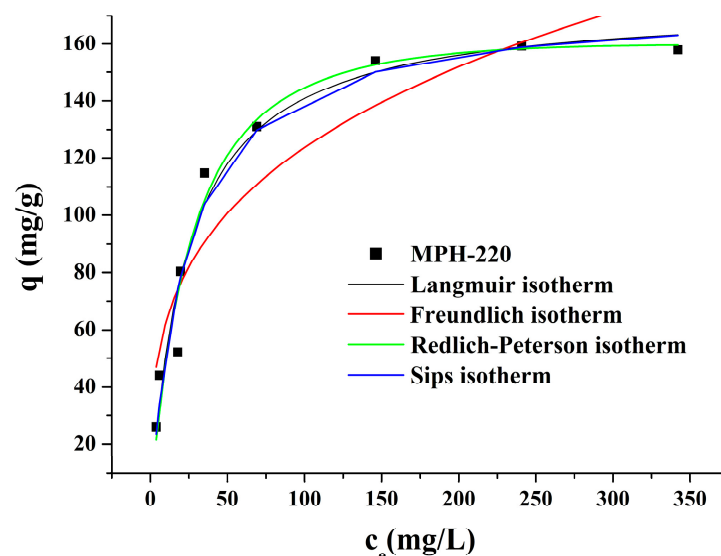


Figure 3. Non-linear fits of isotherm models to the Pb(II) adsorption by MPH-220.

Table 3. Isothermal parameters for Pb(II) sorption on the MPH-220.

Adsorbent MPH-220	
Langmuir isotherm model	
q_m [mg/g]	174.75
K_L [L/mg]	0.04
χ^2	10.85
R^2	0.9678
Freundlich isotherm model	
K_F [(mg/g) (L/mg) ^{1/n}]	31.57
1/n	0.30
χ^2	37.93
R^2	0.8801
Sips isotherm model	
q_m [mg/g]	174.06
K_S [L/mg]	0.04
n_S	1.00
χ^2	11.90
R^2	0.9657
Redlich–Peterson isotherm model	
K_{RP} [L/g]	6.22
a_{RP} [L/mg]	0.02
β	1.07
χ^2	12.65
R^2	0.9665

The correlation coefficient R^2 implies that the three isotherm models had similar values, around 0.96. These similarities are also visible in Figure 3, where the plots of these three isotherm models almost overlap. Moreover, the value of the R^2 coefficient was highest for the Langmuir model, so it can be concluded that this isotherm model provides insight into the nature of the interaction between the MPH-220 and Pb(II) ions. This model implies monolayer chemical sorption onto homogenous active sites of the MPH-220 surface, without synergy between the adsorbed ions. Similar findings were previously reported for Pb(II) ions removal by other hydrochars [4,8,12,15]. According to the obtained isotherms parameters, $K_L < 1$, $K_F > 1$, the 1/n and n_S values were in a range from 0 to 1, and the removal of Pb ions favored the process [17] (Table 3). Based on the Langmuir isotherm, the maximum adsorption capacity (q_m) that could be achieved using MPH-220 was 174.75 mg/g. The removal efficiency of the MPH-220 tested in this paper was comparable to, or even better than, other carbonaceous materials and biomasses previously investigated as Pb(II) sorbents (Table 4).

Table 4. The maximum adsorption capacity of Pb(II) sorption on similar materials.

Adsorbent	q_m [mg/g]	Reference
<i>Phragmites</i> biomass	5.46	[36]
Acid-activated <i>Juniperus procera</i> leaves carbon	30.30	[37]
<i>Azadirachta indica</i> leaves powder	39.7	[38]
Alkali-activated camphor leaves biochar	98.33	[12]
Alkali-activated digested sewage sludge hydrochar	109.30	[4]
Sulfide-modified magnetic pinecone-derived hydrochar	149.33	[15]
Dithiocarbamate-modified bamboo hydrochar	151.51	[8]
Microwave-pyrolyzed canola straw biochar produced at 500 °C	165.00	[16]
MPH-220	174.75	This study
PEI-modified corn stover hydrochar	214.00	[7]
H ₃ PO ₄ -modified corn stover hydrochar	353.40	[7]

3.4. Adsorption Thermodynamic Studies

One of the essential tools for understanding the adsorption mechanisms and the nature of adsorption is thermodynamic study, as shown in Table 5 and Figure S1. The changes in the free Gibbs energy (ΔG°) were negative values, which indicates that Pb(II) sorption was a spontaneous and favorable process at the investigated temperatures. The endothermic nature of the presented sorption was confirmed by a positive ΔH° value. A positive ΔS° implies increased randomness at the solid-liquid interface [33]. Similar findings have been obtained during Pb sorption onto other carbonaceous materials [8,37].

Table 5. Thermodynamic parameters for Pb(II) sorption onto the MPH-220.

T [K]	ln K _c	ΔG° [kJ/mol]	ΔH° [kJ/mol]	ΔS° [J/(mol × K)]	R ²
298.15	10.60	−25.54			
308.15	11.64	−31.41	149.47	586.92	0.9263
318.15	14.41	−37.28			

3.5. Functional Groups—FTIR Analysis

To determine the changes in the chemical structure of the PH-220 before and after NaOH modification, FTIR analysis was performed. According to the FTIR spectra (Figure 4a), the surface functional groups of the PH-220 were changed significantly upon alkali modification.

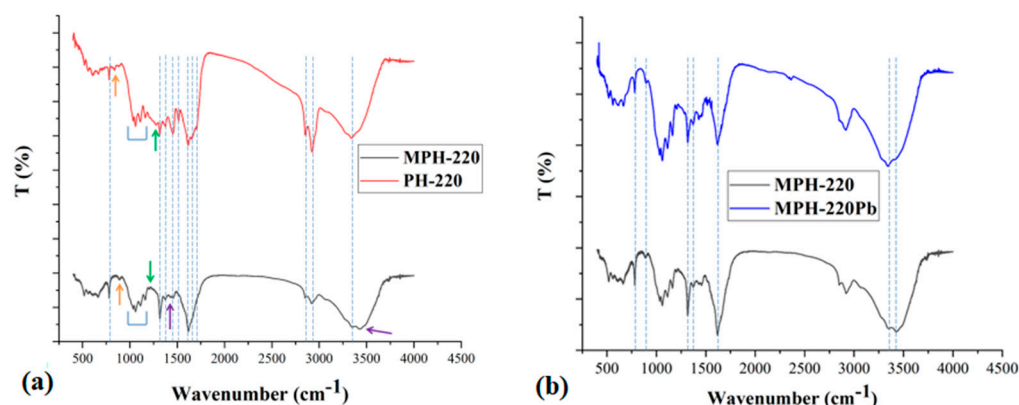


Figure 4. FTIR analysis: (a) hydrochar before and after NaOH modification; (b) modified hydrochar before and after Pb(II) sorption.

The FTIR spectra of the PH-220 showed peaks characteristic for lignocellulosic biomass hydrochars (Figure 4a). The peak at 780 cm^{-1} could be attributed to aromatic C-H deformations [17,18,39]. Furthermore, the peak at 837 cm^{-1} showed the presence of aromatic =C-H bonds [7,16]. The bands at 1034 , 1060 , 1111 , and 1162 cm^{-1} indicated the presence of -C-O and C-O-C bonds, which originated from alcohols, phenols, esters, carboxylic acids and/or ethers, while the sharp peaks at 1315 , 1455 , 1516 and 1615 cm^{-1} confirmed the presence of aromatic rings [3,6,7,13,18,35,39]. In addition, the FTIR spectra of PH-220 also exhibited peaks at 1375 cm^{-1} and 1277 cm^{-1} , which originated from C-O stretch bonds [13,17,35,39], peaks at 1455 cm^{-1} (C-H deformation in the carbohydrates and lignin [17,39]), 1516 cm^{-1} (C=C from the aromatic ring [18,39]), 1648 cm^{-1} (C=O vibration of carboxyl, aldehyde and ketone groups [16,35]), and 1703 cm^{-1} (C=O from cellulose and lignin [7,40]), and peaks at 2851 and 2924 cm^{-1} , which originated from asymmetric and symmetric -C-H valence vibration of CH_3 and CH_2 groups [40–42]. In PH-220, the wide band around 3340 cm^{-1} was attributed to -O-H group stretching vibration from alcohol, phenol, and carboxylic compounds [7,18,40].

As can be seen from Figure 4a, particular changes as a result of alkali modification could be observed. Movements were observed from peak 837 to 890 cm^{-1} (Figure 4a marked with orange arrows) and from peak 1277 to 1206 cm^{-1} (Figure 4a marked with green arrows). These peaks originated from the aromatic =C-H and the C-O bonds, respectively. Peaks reduction and disappearance are highly noticeable for the peaks at 1455, 1516, 1648 and 1703 cm^{-1} . These changes indicated a partial hydrolytic degradation of the lignocellulose structures after modification [39]. Additionally, the intensity of peaks at 2851 and 2924 cm^{-1} was significantly decreased in MPH-220. The observed differences suggest that, during NaOH treatment, methylene and aromatic -C-H groups were partially removed. The same occurrence was observed by Yu et al. [42] during CO_2 activation of char. Two new peaks, which could be observed in the spectrum of the MPH-220 at 1428 and 3423 cm^{-1} (at Figure 4a marked with purple arrows), confirmed the binding of O-H groups to the surface of hydrochars as a result of successful modification [3,13,34,40,41].

The removal performance substantially depended on the surface functional groups of the adsorbents [3]. To investigate the binding mechanisms and differences caused by adsorption of Pb(II), FTIR analysis of the MPH-220 before and after adsorption was performed (Figure 4b). Upon adsorption, the peak at 780 cm^{-1} decreased as a result of interaction with metal ions [17,39]. In addition, the intensity of peaks at 1315 cm^{-1} (originating from the aromatic ring [18]), 1375 cm^{-1} (originating from -C-O [17,39]), and 1615 cm^{-1} (originating from the aromatic ring [7,17]), were reduced after Pb(II) adsorption. Additionally, the peak at 890 cm^{-1} from MPH-220 was slightly shifted to 896 cm^{-1} . These observations suggest that two possible mechanisms for Pb(II) binding were complexation and/or cation- π electron interaction [16,17]. Furthermore, the peak at 3423 cm^{-1} , which was detected only in the MPH-220 sample, disappeared after Pb(II) ions adsorption from aqueous solution. This occurrence suggests that newly formed -O-H groups in the modified PH-220 also participated in the adsorption process.

According to FTIR analysis (Figure 4a), the alkali modification especially affected the aromatic structure and the present of OFG. Therefore, this led to a change in the sorption efficiency. The FTIR results (Figure 4b) confirmed that groups such as aromatic C=C (π electron interaction) and oxygen-containing groups, -C-O and -O-H, played an important role during the adsorption of metal ions on the reactive surface [16,17,39]. The new adsorbent MPH-220 might be beneficial for the adsorption of metal ions, such as Pb(II) ions.

3.6. SEM/EDS of PH-220, MPH-220 and MPH-220Pb

To provide further information about the effect of the NaOH modification process on the PH-220 material structure, the surface morphological structure and elemental mapping of hydrochar samples (PH-220 and MPH-220) were evaluated by SEM/EDS analyses. In addition, SEM/EDS was used to compare the morphological structure of the MPH-220 before and after Pb(II) adsorption.

The surface of the PH-220 displayed an irregular stacking structure with pores of various dimensions (Figure 5). There was a considerable difference in the surface morphology after NaOH modification (Figure 5). The surface structure of the PH-220 was cracked into uneven fragments with new folds, pores, holes and channels. The external structure of the modified hydrochar was changed as a result of carbon chain discontinuity and other reactions that included polycondensation and rearrangement of the residual organics [13]. These irregularities on the MPH-220 structure might be advantageous for ion diffusion and exposure of more active sites for the sorption process [12,42]. The MPH-220 surface after Pb(II) adsorption was spongy with agglomerated particles and floccules without defined porosity.

The EDS spectra of the PH-220, MPH-220 before and after Pb(II) adsorption showed that the main elements were carbon (C) and oxygen (O) (Table S2). The tested samples exhibited average values of C and O higher than 50 and 35%, respectively, indicating that all samples had carbon-rich structures and OFG on the surface [12]. Of the minor elements,

calcium (Ca) was the most presented (about 3%), followed by phosphorus (P, about 1%). Ca as the main metal element was also observed in previous studies of various carbon-rich materials [4,6,12,41]. After adsorption, there was some increase in the Pb amount from 0.00% in PH-220 and MPH-220 to an average value of 4.66% in MPH-220Pb. This result from the EDS analysis suggests that the Pb(II) ions were most likely bound to the adsorbent surface, as was also observed in a previous study on alkali-activated, dewatered, digested sewage sludge hydrochar [4].

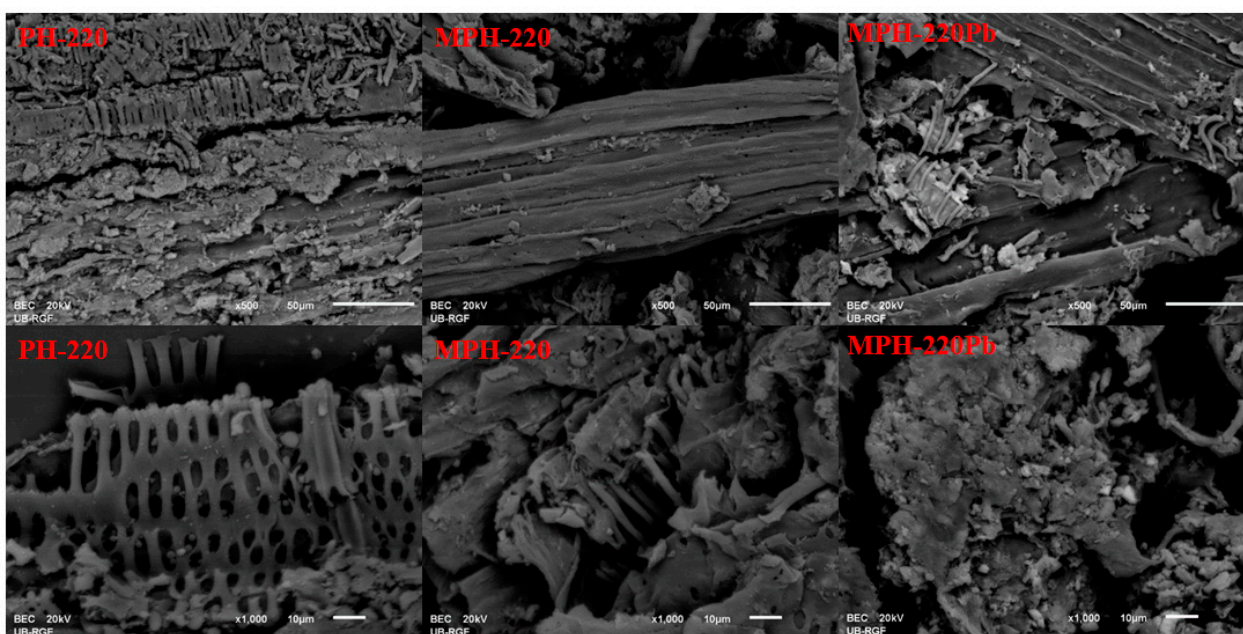


Figure 5. The SEM images of hydrochar, modified hydrochar before and after Pb(II) sorption.

3.7. Possible Pb(II) Adsorption Mechanisms

The summarized results from this study might be useful for better understanding of the nature of the interaction between modified PL hydrochar and Pb(II) ions from aqueous solution. Chemical interaction between the Pb(II) ions and the MPH-220 was confirmed by the kinetic models. As can be concluded from the FTIR analysis (Figure 4), the adsorption of Pb(II) ions was associated with the amount of OFGs on the hydrochar surface due to mutual complexation and π -electron interaction from C=C. These conclusions are in accordance with previous studies [12,17,35]. In order to confirm the ion exchange mechanism the amount of H^+ , Na^+ , K^+ , Mg^{2+} and Ca^{2+} were measured in filtrates before and after Pb(II) sorption at different initial Pb(II) concentrations (Figure 6). In agreement with the EDS result, Ca^{2+} was the predominant cation included in the ion-exchange during the adsorption, followed by Na^+ and Mg^{2+} ions. The total amount of the exchanged cations suggests that ion-exchange was one of the mechanisms that contributed to the removal of the Pb(II) ions by MPH-220.

The determination of pH_{PZC} could be useful to indicate the electrostatic interaction between the adsorbent surface and metal ions from the solution [29]. As can be seen from Figure S2, the pH_{PZC} for MPH-220 was found to be 7.35. Below this pH value, the MPH-220 surface stayed positively charged, and interaction with cations could be reduced. The adsorption of Pb(II) ions onto the MPH-220 surface was performed at pH value $< pH_{PZC}$, which indicates that electrostatic forces were not a dominant mechanism during sorption.

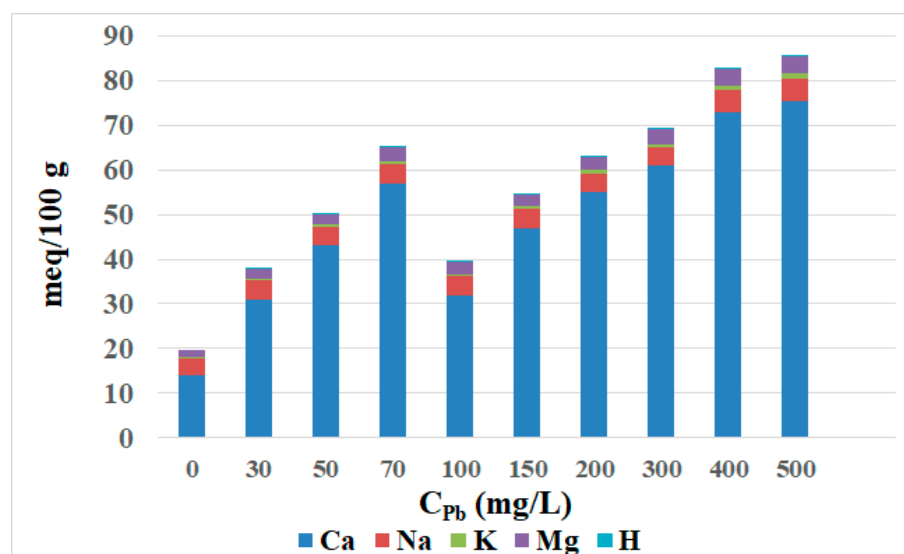


Figure 6. The released cations during ion exchange using MPH-220.

3.8. Stability and Reusability Studies

The amount of oxidized carbon with respect to the total carbon of the hydrochar was calculated to be 0.085 ± 0.003 , which indicated good stability of MPH-220 for the specified use. The adsorption-desorption tests of the MPH-220 in three regeneration cycles are presented in Figure S3. The adsorption capacity decreased from 107.0 to 86.0 mg/g as the number of cycles increased. However, the desorption efficiency of MPH-220 toward Pb(II), around 87%, did not change significantly. A similar trend in the Pb(II) removal efficiency was observed by Li et al. and Zhang et al. during desorption experiments of dithiocarbamate-modified bamboo hydrochar and sulfide-modified magnetic pinecone-derived hydrochar, respectively [8,15]. This observation showed that the tested MPH-220 can be regenerated by HNO_3 and successfully reused for Pb(II) adsorption.

4. Conclusions

In this study, alkali-modified hydrochar from *Paulownia* leaves was used for the removal of Pb(II) from an aqueous solution. To assess the justification for alkali modification, the results of Pb(II) adsorption in the batch system using MPH-220 were compared with the feedstock and corresponding PH. It was found that MPH-220 had a higher removal capacity than its predecessor. The adsorption of Pb(II) onto MPH-220 followed non-linear and linear pseudo-second-order kinetic models. Additionally, the intra-particle model implied that there were two stages in the sorption process. The Langmuir isotherms model best described metal adsorption by MPH-220. That means that monolayer chemical sorption onto the homogenous active site was the most predominant. According to the Langmuir isotherms, the maximum adsorption capacity of the modified PL hydrochar was 174.75 mg/g. Additionally, thermodynamic studies showed that Pb(II) sorption onto MPH-220 was a favorable and spontaneous process with negative change in the Gibbs free energy at all investigated temperatures. The FTIR showed differences in functional groups of the surface which might be a consequence of NaOH treatment. The methylene and aromatic -C-H groups were partially removed, while new -O-H groups were detected. Additionally, the FTIR showed that the adsorption of the Pb(II) ions was mostly related to OFG, =C-H, and C=C groups on the MPH-220 surface. The SEM images also showed newly formed fragments at the surface of the modified hydrochar. After the Pb(II) sorption, the surface was more spongy. The EDS analysis revealed that the main elements in all the tested samples were C and O. These results confirmed the presence of OFG groups and carbon-rich structures. In summary, there was an improvement in the structural characteristics and adsorption efficiency of MPH compared to PL and PH. However, it should be emphasized

here that the PL and its PH also showed high values of the Pb(II) removal coefficient from the aqueous solution (of 73.44 mg/g and 82.37 mg/g, respectively), so they can also be assessed in more detail as potential sorbents. Certainly, further research in this direction should be carried out, especially in terms of the assessment of the stability of these sorbents. Furthermore, considering the availability of PL biomass, low-cost, eco-friendly PH and MPH have the potential to be used as efficient adsorbents of Pb(II) from wastewaters.

Supplementary Materials: The following supporting information can be downloaded at: <https://www.mdpi.com/article/10.3390/pr11051327/s1>, Figure S1: The adsorption thermodynamic plot of Pb ions removal with MPH-220; Figure S2: The point of zero charges (pHPZC) of the MPH-220 surface; Figure S3: Ad-sorption and desorption cycle performance of MPH-220; Table S1: Kinetic parameters of PFO and PSO non-linear models for Pb(II) adsorption onto MPH-220, CPb = 200 mg/L; Table S2: The average surface chemical composition (wt%) determined by EDS analysis.

Author Contributions: Conceptualization, M.K.; methodology, M.S. and J.P.; software, M.E.; validation, M.E. and J.D.; formal analysis, M.S. and J.P.; investigation, M.K.; resources, J.P.; data curation, J.D.; writing—original draft preparation, M.K.; writing—review and editing, M.S. and J.P.; visualization, M.S.; supervision, M.E. Please turn to the CRediT taxonomy <https://img.mdpi.org/data/contributor-role-instruction.pdf> (accessed on 24 February 2023) for explanation of terms. All authors have read and agreed to the published version of the manuscript.

Funding: This research received no external funding.

Data Availability Statement: Not applicable.

Acknowledgments: The authors acknowledge the Serbian Ministry of Education, Science and Technological Development for financial support (contract no. 451-03-47/2023-01/200023).

Conflicts of Interest: The authors declare no conflict of interest. The funders had no role in the design of the study; in the collection, analyses, or interpretation of data; in the writing of the manuscript; or in the decision to publish the results.

References

1. Gallifuoco, A. A new approach to kinetic modeling of biomass hydrothermal carbonization. *ACS Sustain. Chem. Eng.* **2019**, *7*, 13073–13080. [\[CrossRef\]](#)
2. Holliday, M.C.; Parsons, D.R.; Zein, S.H. Microwave-Assisted Hydrothermal Carbonisation of Waste Biomass: The Effect of Process Conditions on Hydrochar Properties. *Processes* **2022**, *10*, 1756. [\[CrossRef\]](#)
3. Rasam, S.; Moraveji, M.K.; Soria-Verdugo, A.; Salimi, A. Synthesis, characterization and absorbability of *Crocus sativus* petals hydrothermal carbonized hydrochar and activated hydrochar. *Chem. Eng. Process* **2021**, *159*, 108236. [\[CrossRef\]](#)
4. Malool, M.E.; Moraveji, M.K.; Shayegan, J. Hydrothermal carbonization of digested sewage sludge coupled with Alkali activation: Integrated approach for sludge handling, optimized production, characterization and Pb(II) adsorption. *J. Taiwan Inst. Chem. E* **2022**, *133*, 104203. [\[CrossRef\]](#)
5. Nguyen, L.H.; Nguyen, X.H.; Nguyen, N.D.K.; Van, H.T.; Thai, V.N.; Le, H.N.; Pham, V.D.; Nguyen, N.A.; Nguyen, T.P.; Nguyen, T.H. H₂O₂ modified-hydrochar derived from paper waste sludge for enriched surface functional groups and promoted adsorption to ammonium. *J. Taiwan Inst. Chem. E* **2021**, *126*, 119–133. [\[CrossRef\]](#)
6. Lang, J.; Matějová, L.; Cuentas-Gallegos, A.K.; Lobato-Peralta, D.R.; Ainassaari, K.; Gómez, M.M.; Solís, J.L.; Mondal, D.; Keiski, R.L.; Cruz, G.J.F. Evaluation and selection of biochars and hydrochars derived from agricultural wastes for the use as adsorbent and energy storage materials. *J. Environ. Chem. Eng.* **2021**, *9*, 105979. [\[CrossRef\]](#)
7. Jiang, Q.; Xie, W.; Han, S.; Wang, Y.; Zhang, Y. Enhanced adsorption of Pb(II) onto modified hydrochar by polyethyleneimine or H₃PO₄: An analysis of surface property and interface mechanism. *Colloids Surf. A* **2019**, *583*, 123962. [\[CrossRef\]](#)
8. Li, B.; Guo, J.-Z.; Liu, J.-L.; Fang, L.; Lv, J.-Q.; Lv, K. Removal of aqueous-phase lead ions by dithiocarbamate modified hydrochar. *Sci. Total Environ.* **2020**, *714*, 136897. [\[CrossRef\]](#)
9. Nguyen, T.-B.; Truong, Q.-M.; Chen, C.-W.; Doong, R.; Chen, W.-H.; Dong, C.-D. Mesoporous and adsorption behavior of algal biochar prepared via sequential hydrothermal carbonization and ZnCl₂ activation. *Bioresour. Technol.* **2022**, *346*, 126351. [\[CrossRef\]](#)
10. Qu, J.; Lin, X.; Liu, Z.; Liu, Y.; Wang, Z.; Liu, S.; Meng, Q.; Tao, Y.; Hu, Q.; Zhang, Y. One-pot synthesis of Ca-based magnetic hydrochar derived from consecutive hydrothermal and pyrolysis processing of bamboo for high-performance scavenging of Pb(II) and tetracycline from water. *Bioresour. Technol.* **2022**, *343*, 126046. [\[CrossRef\]](#)

11. Elsayed, I.; Madduri, S.; El-Giar, E.M.; Hassan, E.B. Effective removal of anionic dyes from aqueous solutions by novel polyethylenimine-ozone oxidized hydrochar (PEI-OzHC) adsorbent. *Arab. J. Chem.* **2022**, *15*, 103757. [[CrossRef](#)]
12. Wang, C.; Wang, H.; Cao, Y. Pb(II) sorption by biochar derived from *Cinnamomum camphora* and its improvement with ultrasound-assisted alkali activation. *Colloids Surf. A* **2018**, *556*, 177–184. [[CrossRef](#)]
13. Tu, W.; Liu, Y.; Xie, Z.; Chen, M.; Ma, L.; Du, G.; Zhu, M. A novel activation-hydrochar via hydrothermal carbonization and KOH activation of sewage sludge and coconut shell for biomass wastes: Preparation, characterization and adsorption properties. *J. Colloid Interface Sci.* **2021**, *593*, 390–407. [[CrossRef](#)] [[PubMed](#)]
14. He, X.; Zhang, T.; Xue, Q.; Zhou, Y.; Wang, H.; Bolan, N.S.; Jiang, R.; Tsang, D.C.W. Enhanced adsorption of Cu(II) and Zn(II) from aqueous solution by polyethylenimine modified straw hydrochar. *Sci. Total Environ.* **2021**, *778*, 146116. [[CrossRef](#)]
15. Zhang, Y.; Qu, J.; Yuan, Y.; Song, H.; Liu, Y.; Wang, S.; Tao, Y.; Zhao, Y.; Li, Z. Simultaneous scavenging of Cd(II) and Pb(II) from water by sulfide-modified magnetic pinecone-derived hydrochar. *J. Clean. Prod.* **2022**, *341*, 130758. [[CrossRef](#)]
16. Nzediegwu, C.; Naeth, M.A.; Chang, S.X. Lead(II) adsorption on microwave-pyrolyzed biochars and hydrochars depends on feedstock type and production temperature. *J. Hazard. Mater.* **2021**, *412*, 125255. [[CrossRef](#)]
17. Petrović, J.; Stojanović, M.; Milojković, J.; Petrović, M.; Šoštarić, T.; Laušević, M.; Mihajlović, M. Alkali modified hydrochar of grape pomace as a perspective adsorbent of Pb²⁺ from aqueous solution. *J. Environ. Manag.* **2016**, *182*, 292–300. [[CrossRef](#)]
18. Koprivica, M.; Petrović, J.; Ercegović, M.; Simić, M.; Milojković, J.; Šoštarić, T.; Dimitrijević, J. Improvement of combustible characteristics of *Paulownia* leaves via hydrothermal carbonization. *Biomass Convers. Biorefin.* **2022**. [[CrossRef](#)]
19. Lagergren, S. Zur Theorie der Sogenannten Adsorption Gelöster Stoffe. *K. Sven. Vetensk. Handl.* **1898**, *24*, 1–39. [[CrossRef](#)]
20. Tran, H.N.; You, S.-J.; Hosseini-Bandegharaei, A.; Chao, H.-P. Mistakes and inconsistencies regarding adsorption of contaminants from aqueous solutions: A critical review. *Water Res.* **2017**, *120*, 88–116. [[CrossRef](#)]
21. Ibrahim, A.A.; Salama, R.S.; El-Hakam, S.A.; Khder, A.S. Synthesis of 12-tungstophosphoric acid supported on Zr/MCM-41 composite with excellent heterogeneous catalyst and promising adsorbent of methylene blue. *Colloids Surf.* **2021**, *631*, 127753. [[CrossRef](#)]
22. Ho, Y.S.; McKay, G. Pseudo-second order model for sorption processes. *Process Biochem.* **1999**, *34*, 451–465. [[CrossRef](#)]
23. Weber, W.; Morris, J. Kinetics of adsorption on carbon from solution. *J. Sanit. Eng. Div.* **1963**, *89*, 31–60. [[CrossRef](#)]
24. Langmuir, I. The adsorption of gases on plane surfaces of glass, mica and platinum. *J. Am. Chem. Soc.* **1918**, *40*, 1361–1368. [[CrossRef](#)]
25. Freundlich, H.M.F. Over the adsorption in solution. *J. Phys. Chem.* **1906**, *57*, 384–470. [[CrossRef](#)]
26. Sips, R. On the structure of a catalyst surface. *J. Chem. Phys.* **1948**, *16*, 490–495. [[CrossRef](#)]
27. Redlich, O.J.; Peterson, D.L. A useful adsorption isotherm. *J. Phys. Chem.* **1959**, *63*, 1024. [[CrossRef](#)]
28. Petrović, J.; Ercegović, M.; Simić, M.; Kalderis, D.; Koprivica, M.; Milojković, J.; Radulović, D. Novel Mg-doped pyro-hydrochars as methylene blue adsorbents: Adsorption behavior and mechanism. *J. Mol. Liq.* **2023**, *376*, 121424. [[CrossRef](#)]
29. Petrović, M.; Šoštarić, T.; Stojanović, M.; Milojković, J.; Mihajlović, M.; Stanojević, M.; Stanković, S. Removal of Pb²⁺ ions by raw corn silk (*Zea mays* L.) as a novel biosorbent. *J. Taiwan Inst. Chem. Eng.* **2016**, *58*, 407–416. [[CrossRef](#)]
30. Milonjić, S. A consideration of the correct calculation of thermodynamic parameters of adsorption, short communication. *J. Serb. Chem. Soc.* **2007**, *72*, 1363–1367. [[CrossRef](#)]
31. Chen, D.; Yu, X.; Song, C.; Pang, X.; Huang, J.; Li, Y. Effect of pyrolysis temperature on the chemical oxidation stability of bamboo biochar. *Bioresour. Technol.* **2016**, *218*, 1303–1306. [[CrossRef](#)] [[PubMed](#)]
32. Salama, R.S.; El-Hakam, S.A.; Samra, S.E.; El-Dafrawy, S.M.; Ibrahim, A.A.; Ahmed, A.I. Synthesis, characterization of titania supported on mesoporous MCM-41 and its application for the removal of methylene blue. *Delta Univ. Sci. J.* **2022**, *5*, 321–339. [[CrossRef](#)]
33. Thamer, B.M.; Aldalbahi, A.; Moydeen, M.A.; Al-Enizi, A.; El-Hamshary, H.; El-Newehy, M. Fabrication of functionalized electrospun carbon nanofibers for enhancing lead-ion adsorption from aqueous solutions. *Sci. Rep.* **2019**, *9*, 19467. [[CrossRef](#)]
34. Zhu, S.; Chen, Y.; Khan, M.A.; Xu, H.; Wang, F.; Xia, M. In-Depth Study of Heavy Metal Removal by an Etidronic Acid-Functionalized Layered Double Hydroxide. *ACS Appl. Mater. Interfaces* **2022**, *14*, 7450–7463. [[CrossRef](#)] [[PubMed](#)]
35. Simić, M.; Petrović, J.; Šoštarić, T.; Ercegović, M.; Milojković, J.; Lopičić, Z.; Kojić, M. A Mechanism Assessment and Differences of Cadmium Adsorption on Raw and Alkali-Modified Agricultural Waste. *Processes* **2022**, *10*, 1957. [[CrossRef](#)]
36. Amro, A.N.; Abhary, M.K.; Shaikh, M.M.; Ali, S. Removal of Lead and Cadmium Ions from Aqueous Solution by Adsorption on a Low-Cost *Phragmites* Biomass. *Processes* **2019**, *7*, 406. [[CrossRef](#)]
37. Ali, I.H.; Mesfer, M.K.A.; Khan, M.I.; Danish, M.; Alghamidi, M.M. Exploring Adsorption Process of Lead (II) and Chromium (VI) Ions from Aqueous Solutions on Acid Activated Carbon Prepared from *Juniperus procera* Leaves. *Processes* **2019**, *7*, 217. [[CrossRef](#)]
38. Elkhaleefa, A.; Ali, I.H.; Brima, E.I.; Shigidi, I.; Elhag, A.B.; Karama, B. Evaluation of the Adsorption Efficiency on the Removal of Lead(II) Ions from Aqueous Solutions Using *Azadirachta indica* Leaves as an Adsorbent. *Processes* **2021**, *9*, 559. [[CrossRef](#)]
39. Mihajlović, M.; Petrović, J.; Kragović, M.; Stojanović, M.; Milojković, J.; Lopičić, Z.; Koprivica, M. Effect of KOH activation on hydrochar surface: FT-IR analysis. *Rad. Appl.* **2017**, *2*, 65–67. [[CrossRef](#)]
40. Teng, F.; Zhang, Y.; Wang, D.; Shen, M.; Hu, D. Iron-modified rice husk hydrochar and its immobilization effect for Pb and Sb in contaminated soil. *J. Hazard. Mater.* **2020**, *398*, 122977. [[CrossRef](#)]

41. Ahmad, S.; Zhu, X.; Wang, Q.; Wei, X.; Zhang, S. Microwave-assisted hydrothermal treatment of soybean residue and chitosan: Characterization of hydrochars and role of N and P transformation for Pb(II) removal. *J. Anal. Appl. Pyrolysis* **2021**, *160*, 105330. [[CrossRef](#)]
42. Yu, J.; Tang, T.; Cheng, F.; Huang, D.; Martin, J.L.; Brewer, C.E.; Grimm, R.L.; Zhou, M.; Luo, H. Waste-to-wealth application of wastewater treatment algae-derived hydrochar for Pb(II) adsorption. *MethodsX* **2021**, *8*, 101263. [[CrossRef](#)] [[PubMed](#)]

Disclaimer/Publisher's Note: The statements, opinions and data contained in all publications are solely those of the individual author(s) and contributor(s) and not of MDPI and/or the editor(s). MDPI and/or the editor(s) disclaim responsibility for any injury to people or property resulting from any ideas, methods, instructions or products referred to in the content.